He metastable density in a double layer formed by a diameter discontinuity in a positive column

James M. Williamson[1] and Biswa N. Ganguly[2]
[1]*Innovative Scientific Solutions, Inc., 2766 Indian Ripple Road, Dayton, Ohio 45440-3638*
[2]*Air Force Research Laboratory, Wright-Patterson Air Force Base, Ohio 45433-7919*
(Received 15 March 2001; published 28 August 2001)

The population density profile of triplet metastable He $(2\,^3S_1)$ is measured in the multiple space-charge (double) layer formed at an abrupt transition of the tube diameter in a positive column discharge. The double layer is formed at the transition from a 2.6 cm diameter to a 0.6 cm diameter tube in a static pressure discharge. The line integrated He $2\,^3S_1$ population density profile in the double-layer region is determined by diode-laser absorption. The triplet metastable density profiles are measured with discharge currents of 1, 2, and 5 mA at 1 Torr pressure for both polarity conditions: (a) when the cathode end of the discharge is in the large diameter tube and (b) when the anode end of the discharge is in the large diameter tube. The diode-laser absorption profiles show enhanced production of triplet metastable He $2\,^3S_1$ in the double-layer region as compared to the unperturbed positive column (0.6 cm diameter) with the magnitude being strongly dependent on the discharge polarity.

DOI: 10.1103/PhysRevE.64.036403 PACS number(s): 52.40.Kh, 52.40.Hf, 52.70.Kz

I. INTRODUCTION

A double or multiple space-charge layer [1] is a localized region of plasma created by adjacent, oppositely charged space-charge layers. This region, as a whole, is neutral but has an internal electric field [2,3] that can accelerate charged particles through the double layer [2–5]. Double layers have been produced in plasmas for many years; they can form as a result of: (a) current limitation in a uniform cross-section plasma, (b) a plasma constriction due to an abrupt change in cross section, (c) a potential difference between two plasmas, or (d) biasing of an anodic electrode above the ionization potential of the neutral gas [1,6–9]. It has been suggested that double layers may be important with regard to current saturation in a gas laser discharge [10], as well as charged particle acceleration in aurora borealis and solar flares [8,11].

A double layer forms in a gas discharge at an abrupt transition of the tube diameter in a positive column to satisfy current continuity [6,7]. The double layer formed at an abrupt diameter change is the result of the transition between areas of plasma with different characteristics such as electron temperature and electron density, which are functions of the discharge tube diameter and current density. Electron densities, electron energy distribution functions, and plasma potentials in the vicinity of such double layers have previously been measured [12–14], but measurements in the double layer have been found to be difficult [8]. A recent study conducted by our group demonstrated that population densities of triplet metastable He can be conveniently and accurately measured in glow discharges using diode-laser absorption [15]. Since absorption measurements are laser based, a very high spatial resolution can be achieved without the disadvantage of perturbing the double layer as in the case of Langmuir probe measurements [1].

In the present paper, we investigated a multiple space-charge (double) layer formed at an abrupt diameter transition in a sealed (constant number density, static gas fill) He discharge cell. The population density of triplet metastable He was measured through the region of the double layer by diode-laser absorption. Using this technique, the population density of triplet metastable He in the region of the double layer was profiled. The change in triplet metastable He population density in the double-layer region when the cathode end of the discharge was in the large diameter tube was measured and compared to that when the anode end of the discharge was in the large diameter tube. The reduced electric field, E/n, (E is electric field and n is number density) could be determined from these profiles in the region of the double layer since the change in triplet metastable He density follows the change in the local reduced electric field and electron density [16].

II. EXPERIMENT

A diagram of the experimental arrangement is shown in Fig. 1. To form the double layer, the discharge cell consists of two areas of larger diameter tubing connected by a length of smaller diameter tubing. The Pyrex cell is constructed of two concentric tubes of different diameters. The inner, smaller diameter tube (8 mm o.d., 6 mm i.d., 10 cm length) is sealed inside the larger (30 mm o.d., 26 mm i.d., 40 cm length) diameter tube such that the larger diameter tube is divided by a seal barrier and the discharge is continuous only through the inner, smaller diameter tube. The 2.5 cm cup electrodes are equidistant from the inner tube, on either side of the seal barrier, as shown in the diagram. The diode-laser output enters and exits the discharge cell through opposed 2.5 cm diameter windows. The windows are positioned such that they are centered ~3 mm from the end of the smaller diameter inner tube. The discharge cell was baked out under high vacuum, filled with ultrahigh purity He (99.999%) to 1 Torr pressure and then sealed. A constant voltage power supply with 50 kΩ ballast resistor powered the discharge and was adjusted to maintain discharge currents of 1, 2, and 5 mA used in this study.

The details of the measurement of metastable He density in glow discharges by diode-laser absorption spectroscopy have been given previously [15]. A Spectra Diode Labs SDL

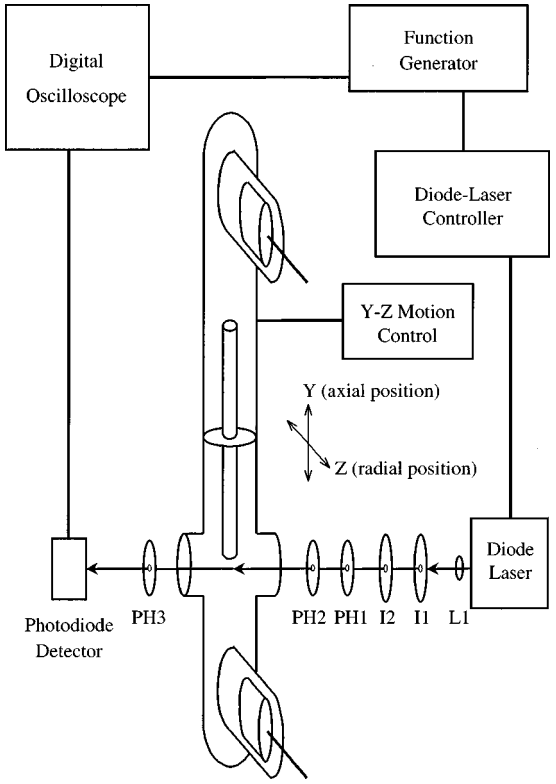

FIG. 1. Schematic diagram of the experimental apparatus (PH1, 2, 3 are pinholes, I1, 2 are iris diaphragms, and L1 is an aspheric lens). Discharge cell is mounted on two-axis translation stages for axial and radial motion of the cell (see text for details).

6702 DBR laser operating with a tunable output around 1083 nm near the He $2\,^3S_1 \rightarrow 2\,^3P_{2,1,0}$ transitions was used for the laser absorption measurements. To define the spatial resolution and reduce the laser power in the discharge cell, the laser output was collimated with an aspherical lens ($L1$ in Fig. 1) and then passed through a series of iris diaphragms and 0.2 and 0.5 mm pinholes ($I1,2$ and $PH1,2$, respectively). After exiting the discharge and passing through a final 0.5 mm pinhole, $PH3$, the laser output absorption was detected by an $In_xGa_{x-1}As$ photodiode. This final pinhole reduced the background signal from stray light and plasma emission. The laser wavelength was scanned by modulating the diode current with a sawtooth ramp from the function generator. A digital oscilloscope (LeCroy 9354C) synchronized to the wavelength sweep by the function generator, was used for signal capture and averaging of the $In_xGa_{x-1}As$ photodiode detector output. The averaged wave forms were then sent to a personal computer for signal processing and analysis.

The metastable $2\,^3S_1$ He spatial profiles were obtained by scanning the discharge cell relative to the laser. For scanning the discharge cell, the cell was mounted on a motorized *Y-Z* translation stage that could be stepped in 1 μm increments in either direction. For axial profiles, the radial *Z* position in the cell was held fixed at the center of the inner tube, while the axial *Y* position was scanned within the viewing limits of the side windows on the discharge cell—roughly from 7 mm inside the inner tube to 10 mm outside the tube (the laser path defined the *X* axis). Radial profiles were obtained by scanning the *Z* position at fixed axial *Y* positions. Spatial profiles of the metastable He density were obtained by measuring the laser transmission signal through the discharge cell at each axial or radial position.

III. ANALYSIS

A detailed description of the analysis of the data obtained from diode-laser absorption measurements can be found elsewhere [15]. Only a brief discussion will be given here. According to Beer's Law, the intensity of the transmitted laser at frequency ν, after absorption by metastable He is given by [17]

$$I_t(\nu) = I_0(\nu) e^{-\sigma(\nu) N l}, \tag{1}$$

where $I_0(\nu)$ is the intensity of incident light, $\sigma(\nu)$ is the absorbtion cross section (cm^{-2}), N is the number density of metastable He (cm^{-3}), and l is the path length through the discharge (cm). With an index of refraction of one, the absorption cross section, $\sigma(\nu)$, is given by [18]

$$\sigma(\nu) = A_{21} \frac{\lambda^2}{8\pi} g(\nu) \frac{g_2}{g_1}, \tag{2}$$

where λ is the wavelength, g_1 and g_2 are the lower and upper state degeneracies $(=2J+1)$, respectively, and $g(\nu)$ is an area-normalized Doppler line-shape function. The spontaneous emission rate A_{21} was taken from Weise, Smith, and Glennon [19] and is $1.022 \times 10^7\ s^{-1}$. The area-normalized Doppler line-shape function is [18]

$$g(\nu) = \sqrt{\frac{4 \ln 2}{\pi}} \frac{1}{\Delta_D} \exp\left[-4 \ln 2 \left(\frac{\nu - \nu_0}{\Delta_D} \right)^2 \right], \tag{3}$$

where Δ_D is the full width at half maximum Doppler linewidth and ν_0 is the line center frequency of the transition. Using Eqs. (2) and (3) in Eq. (1), the metastable He density can be determined. However, because the metastable He number density is not uniform in the discharge [20], the line-integrated density, Nl, is obtained from the laser absorption measurements.

As described in the Sec. II, the metastable $2\,^3S_1$ He density axial profile in the region of the double layer was measured by stepping the discharge cell in the cell-axial direction (*Y* axis), perpendicular to the diode-laser direction (*X* axis) while holding the cell-radial (*Z* axis) position constant at the center of the inner smaller diameter tube. Metastable He absorption measurements were obtained inside and outside the smaller diameter tube, on both sides of the double layer formed at the abrupt transition in tube diameter. Three scans were recorded at each axial cell position: (1) the metastable He absorption spectrum (I_t), (2) the incident laser intensity through the cell with no discharge (I_0), and (3) a background signal scan with the discharge on and the laser blocked (I_0). The background signal scan measures the signal at the detector from the plasma-induced emission and any detector noise. The net transmission signal of the discharge is then $(I_t - I_b)/I_0$.

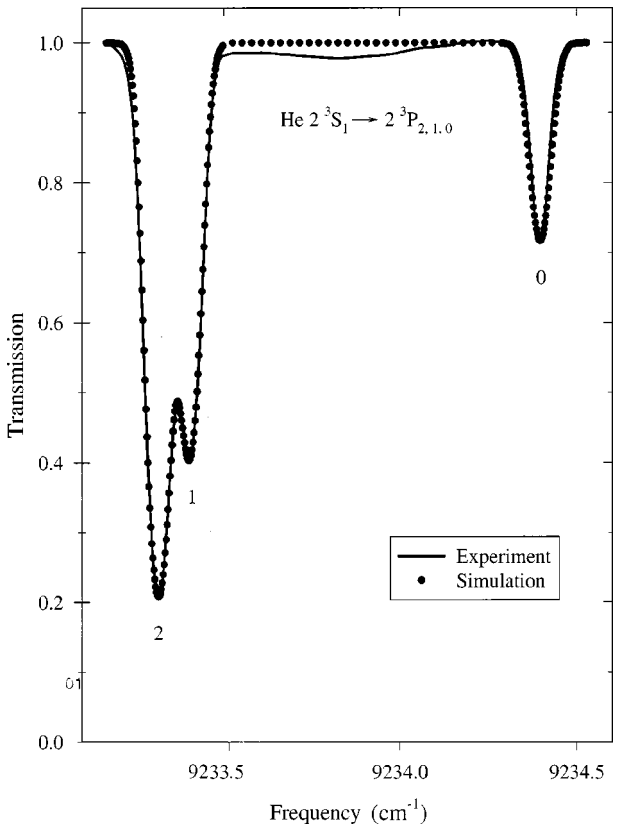

FIG. 2. Absorption spectrum of the $2\,^3S_1 \rightarrow 2\,^3P_{2,1,0}$ transitions in metastable He. Solid line is an experimental spectrum and the dotted line is a fit to the experimental spectrum.

A typical transmission spectrum of metastable He in the region of the $2\,^3S_1 \rightarrow 2\,^3P_{2,1,0}$ transition is shown in Fig. 2. The spectrum consists of transitions from the lower state $J''=1$ level to each of the $J'=2$, 1, or 0 levels of the excited state with intensity ratios equal to the $2J'+1$ statistical weight (5:3:1). The line-integrated metastable He population density is obtained from the transmission spectrum by a simultaneous fit of Eq. (1) to the three transitions. A simulation of the experimental transmission spectrum with the simultaneously fit line-integrated population densities Nl is shown in Fig. 2. The Doppler width Δ_D used in the fit of the three lines was determined from the resolved $2\,^3S_1 \rightarrow 2\,^3P_0$ transition.

IV. RESULTS AND DISCUSSION

Figure 3 shows two images of the plasma emission from the double layer, formed at the abrupt diameter transition, photographed along the laser axis (X axis) through the side window with no optical filters, i.e., total light emission. The images are close-up views of the plasma emission at the tube diameter transition, with the smaller diameter tube (0.6 cm) on the left and the larger diameter tube (2.6 cm) on the right in both images. The two images were obtained under the same cell conditions (1 Torr He, 2 mA) but with the electrode polarities reversed in the two images. In the image on the left side [Fig. 3(a)] the cathode is in the larger diameter section of the transition (right side of image), while [Fig. 3(b)] in the image on the right side the anode is in the larger diameter section of the transition. In general, the plasma

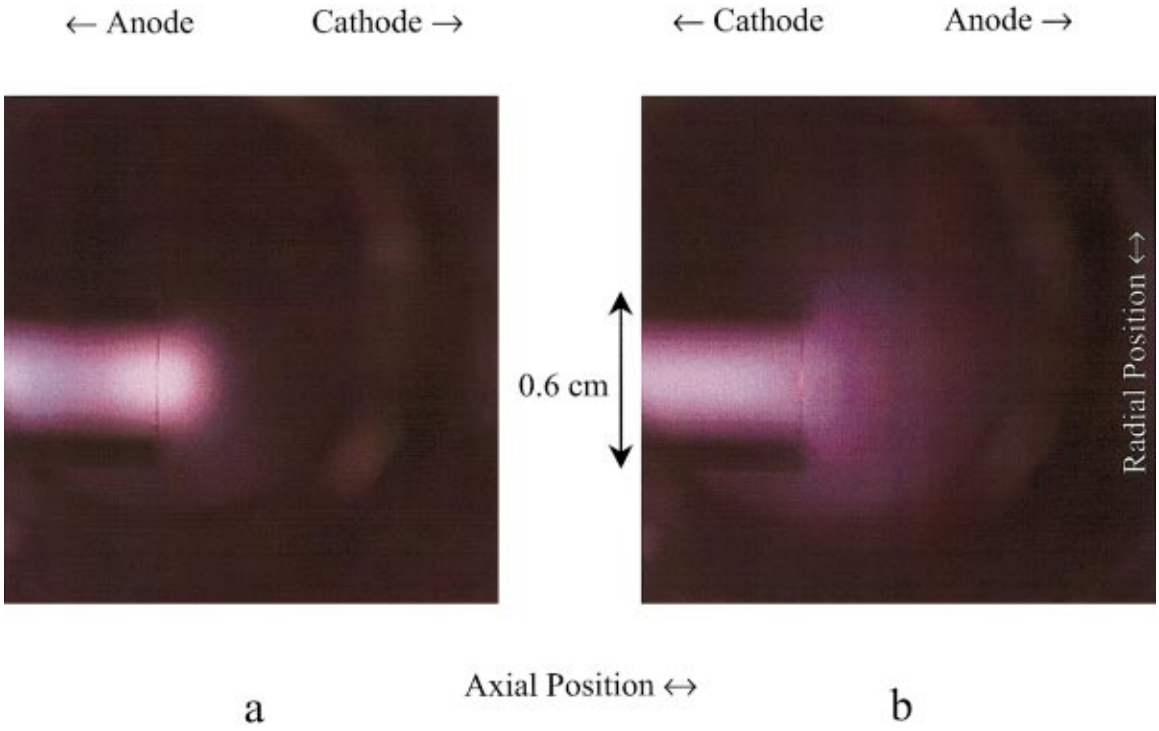

FIG. 3. (Color) Images of the discharge emission from the double-layer region at the abrupt tube diameter transition. (a) Image of the plasma emission with the cathode in the wide (2.6 cm) section of the tube diameter transition. (b) Image of the plasma emission with the anode in the wide (2.6 cm) section of the tube diameter transition. The cell pressure and discharge current were 1 Torr He and 2 mA, respectively.

emission is brighter in the small diameter tube (higher current density and higher E/n). The plasma emission in the two images differs in the transition from the bright region in the small diameter tube to the dim region in the large diameter tube. For the case where the cathode side is in the wide section [Fig. 3(a)], the bright emission protudes from the small diameter tube into the large diameter tube, appearing to be well delineated with a hemispherical shape. The bright protusion extends ~0.3–0.4 cm into the larger tube. For the reverse polarity condition where the anode is in the wide section [Fig. 3(b)], the transition of the bright emission is not well delineated and appears to ''fan out'' from the smaller tube, gradually diminishing with distance from the smaller diameter tube.

Double layers formed at abrupt tube diameter changes or constrictions have been studied previously for the case where the cathode is in the larger diameter tube section and the anode is in the smaller diameter tube section [6,12,13,21]. In the image in Fig. 3(a), the cathode is in the larger diameter section. A region of bright plasma, the so-called ''plasma sac'' [6,13], protudes from the smaller diameter section into the large diameter section. The transition of the plasma emission intensity is sharp, and the location of the double layer is visible when the cathode is in the larger diameter section [12,13]. However, for the reverse discharge polarity (anode in the wide section), as in Fig. 3(b), the change in plasma emission intensity is more gradual; neither the plasma sac nor the double layer is visible.

The metastable He $2\,^3S_1$ line-integrated, population density axial profiles with 1, 2, and 5 mA discharge currents for the two electrode polarities are shown in Figs. 4 and 5. In Fig. 4 the cathode is in the larger diameter section [electrode polarity in Fig. 3(a)] while in Fig. 5 the anode is in the larger diameter section [electrode polarity in Fig. 3(b)]. The line-integrated population densities in Figs. 4 and 5 were determined from a simultaneous fit to the transmission spectrum at each axial position using Eq. (1), as previously described. Radial profiles of the line-integrated, metastable He $2\,^3S_1$ population densities at selected axial positions outside the smaller diameter tube are shown in Fig. 6. These profiles were also determined by a simultaneous fit to the transmission spectrum using Eq. (1). For the radial profiles, the axial position was held fixed at 1, 2.5, and 4 mm from the tube diameter transition in the wide tube section, and the radial position (Z axis) of the cell was scanned. Each profile in Fig. 6 shows population densities for both electrode polarities; in the curves labeled cathode (solid squares) the cathode was in the larger tube section, and for the curves labeled anode (open squares) the anode was in the larger tube section. The population densities were measured for a discharge current of 2 mA.

The axial population density profiles show an increased population of metastable He $2\,^3S_1$ in the region of the double layer at the tube diameter transition. The metastable He population density enhancement increases with discharge current and is evident in the case of the cathode in the larger diameter tube section (Fig. 4). A small, local increase in the population density appears just past the tube diameter transition with the anode in the wider section (Fig. 5), but the

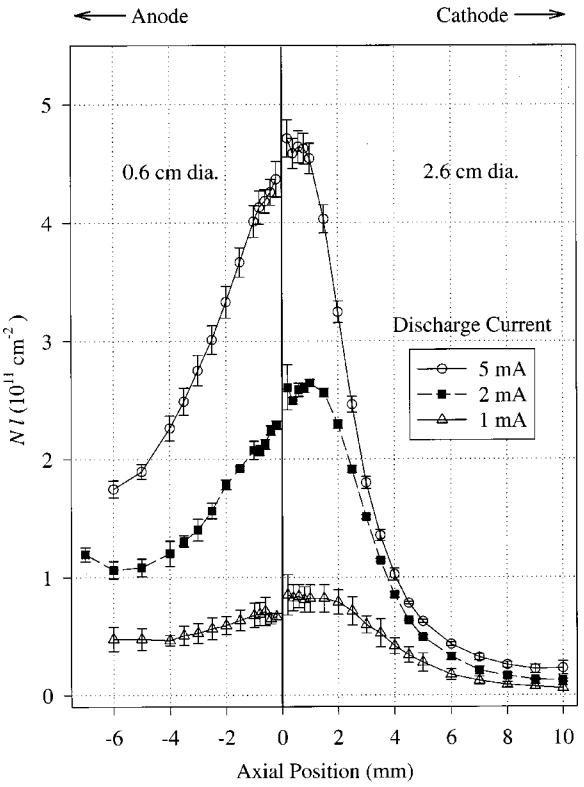

FIG. 4. Line-integrated He $2\,^3S_1$ population density axial profiles in the double layer region for three discharge currents. The electrode polarity corresponds to the polarity used in Fig. 3(a), which has the cathode in the larger diameter section of the discharge. The tube diameter transition is at 0 mm and negative axial positions are inside the smaller diameter tube.

increase is much smaller than with the opposite discharge polarity. The radial profiles are symmetric about the cell center position (0 mm). The metastable He density is sharply peaked and well confined, i.e., the bulk of the population density is within ± 3 mm of the centerline at 1 and 2.5 mm from the tube diameter transition when the cathode is in the wider section. There is less metastable He and the radial profiles are not so peaked when the anode is in the wider tube section. The population density profiles are approximately the same at 4 mm from the tube diameter transition for both cell polarity conditions.

A detailed, nonlocal theoretical model of the discharge and double layer is beyond the scope of the present paper, however, from a simple analysis of the metastable He density measurements, the axial profile of the reduced electric field E/n can be estimated, assuming that the electron energy distribution function (eedf) is in equilibrium with the reduced electric field. The triplet metastable He density can be calculated from a balance equation for the production and loss of metastable He $2\,^3S_1$ atoms [16,22]. The triplet metastable He balance equation at steady state is given by:

$$D\nabla^2 N_{\mathrm{He}*} + k_{\mathrm{exc}} n_e N_{\mathrm{He}} - k_{\mathrm{ion}} n_e N_{\mathrm{He}*} - k_{\mathrm{He}*} N_{\mathrm{He}*}^2 = 0, \quad (4)$$

where $D\nabla^2 N_{\mathrm{He}*}$ is the triplet metastable He diffusion loss to the wall $(= -D(2.405/r)^2 N_{\mathrm{He}*}$, assuming the funda-

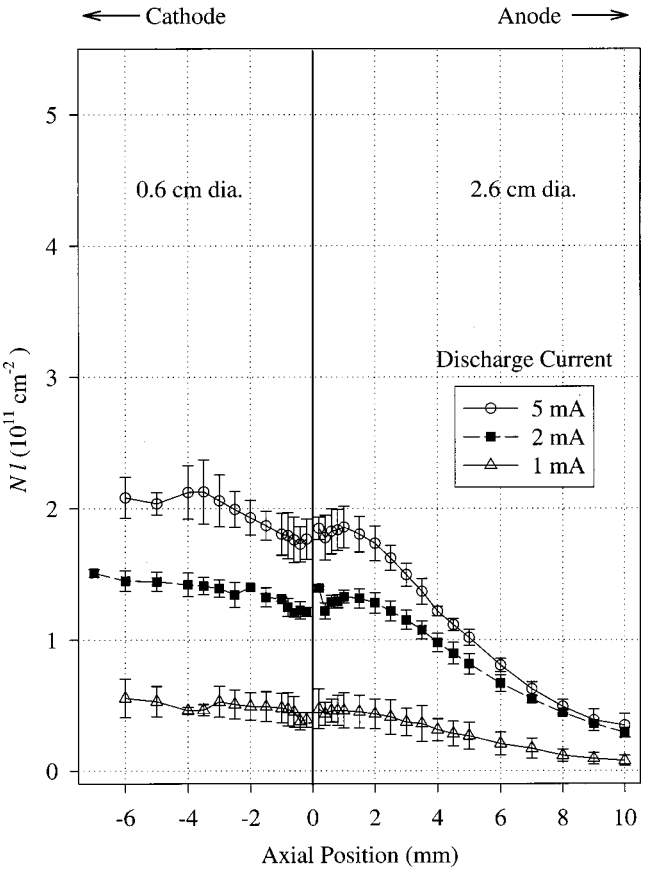

FIG. 5. Line-integrated He $2\,^3S_1$ population density axial profiles in the double-layer region for three discharge currents. The electrode polarity corresponds to the polarity used in Fig. 3(b), which has the anode in the larger diameter section of the discharge. The tube diameter transition is at 0 mm and negative axial positions are inside the smaller diameter tube.

mental diffusion mode). N_{He} and $N_{\mathrm{He}*}$ are the densities of ground and triplet metastable state He, respectively, while n_e is the electron density. k_{exc} is the rate coefficient for the production of triplet metastable He, k_{ion} is the rate coefficient for ionization loss of triplet metastable He, and $k_{\mathrm{He}*}$ is the rate coefficient for the loss of triplet metastable He by triplet-triplet metastable collisions. The triplet metastable He diffusion coefficient was taken from Phelps [23], while the production and loss rate coefficients of Miller, Verdeyen, and Cherrington [16] were used.

The reduced electric field was calculated from the metastable He population line-integrated density profiles in the following manner. The reduced electric field can be determined from the scaling relationships of low-pressure He discharges [24] in the small and large diameter discharge tubes, well away from the tube diameter transition (-6 or -7 mm from the diameter transition, inside the small diameter tube, and $+10$ mm from the transition in the large diameter section; the diameter transition occurred at 0 mm). The electron density inside the small diameter tube was calculated, assuming current continuity, from the electron drift velocity in a He gas discharge [25] and the reduced electric field determined from the scaling relationships [24]. Examination of the discharge images (Fig. 3) and the radial metastable He density profiles (Fig. 6) shows that the majority of the metastable He density is confined to a region $\sim$6 mm wide—the smaller tube diameter—for a distance of 3–4 mm past the tube diameter transition. To simplify the calculation of the reduced electric field from the measured line-integrated metastable He density, a constant electron density and optical path was assumed in Eq. (4) for all points inside the smaller diameter tube and for 4 mm past the tube diameter transition in the wider diameter tube. The excitation (k_{exc}) and ionization (k_{ion}) rate coefficients in Eq. (4) are functions of the reduced electric field [16], while the metastable He loss rate coefficient ($k_{\mathrm{He}*}$) is constant [16,26]. The rate coefficient data set of Miller, Verdeyen, and Cherrington [16] was extrapolated to higher values of reduced electric field by fitting their values to an exponential growth for k_{exc} and an exponential rise to a maximum value for k_{ion}. To compare the measured line-integrated metastable He density with the metastable He number density calculated from Eq. (4), the calculated num-

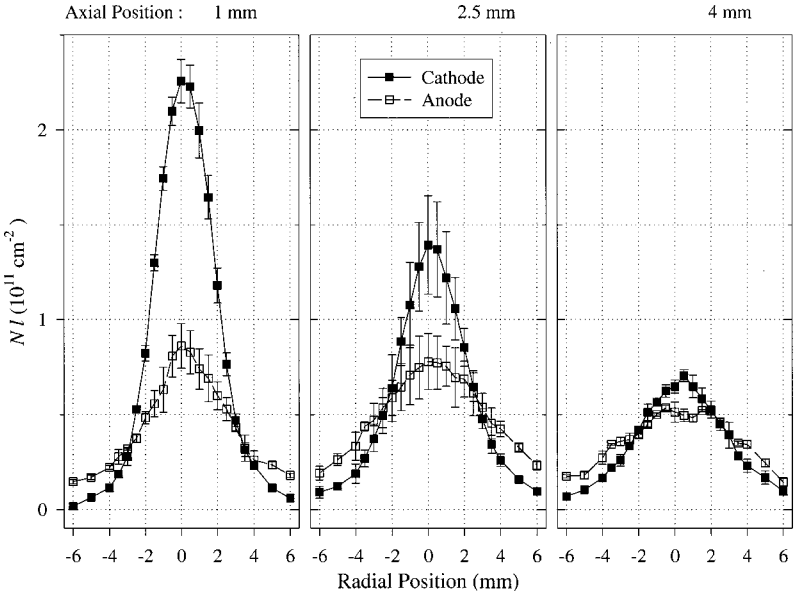

FIG. 6. Line-integrated He $2\,^3S_1$ population density radial profiles in the double layer region at selected axial positions in the larger diameter section of the tube. The solid squares were measured with the cathode in the larger diameter tube section and the open squares with the anode in the larger diameter tube section. The tube diameter transition from the smaller to larger tube is at 0 mm, as in Figs. 4 and 5. The discharge current was 2 mA.

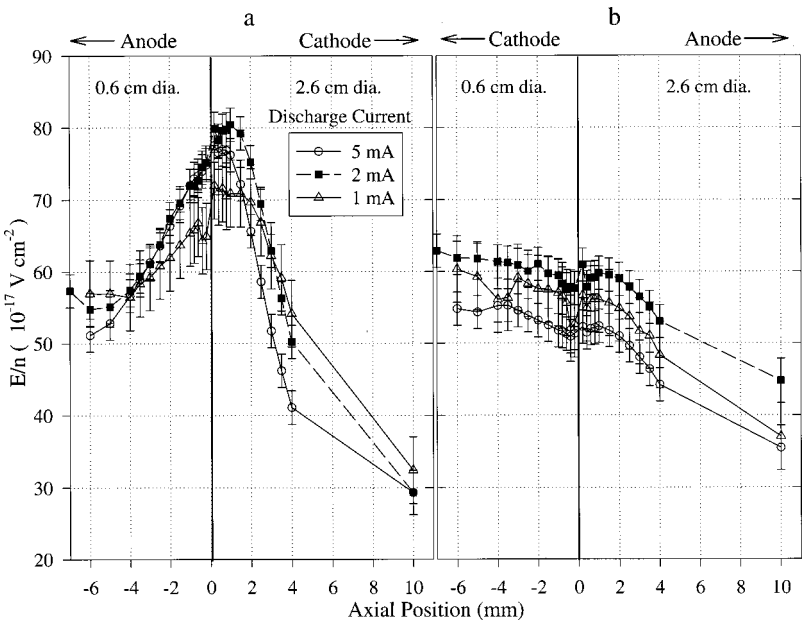

FIG. 7. Reduced electric field axial profiles in the region of the double layer for 1, 2, and 5 mA discharge currents. (a) Reduced electric field with the cathode in the wider tube section. (b) Reduced electric field with the anode in the wider tube section. The tube diameter transition is at 0 mm and negative axial positions are inside the smaller diameter tube.

ber density was transformed to a line-integrated density by multiplication with a derived optical path. The metastable He number density in Eq. (4) was assumed to be the peak of the fundamental diffusion mode distribution (zeroth-order Bessel function). From this distribution, an average-value number density was determined and an optical path length equal to twice the radial position corresponding to this average value was used. The reduced electric field profiles were determined by fitting the measured metastable He densities with Eq. (4) by varying the values of the rate coefficients k_{exc} and k_{ion} (which are functions of the reduced electric field).

The electron density determined using the scaling relationship for the reduced electric field [16] was larger inside the smaller diameter tube than in the larger tube section. Although the electron density is expected to decrease past the diameter transition in the wide section, the change of electron density with axial position is not known. A decrease in the electron density would result in a larger estimated E/n value from the measured metastable He densities; thus, assuming a constant electron density past the diameter transition should result in a lower estimated E/n. Therefore, the estimation of the reduced electric field past the tube diameter transition in the region of the double layer, assuming a constant electron density rather than a decreasing electron density, is expected to be a lower bound. A decreasing electron density would result in a greater enhancement in the estimated reduced electric-field axial profile. The data points at $+10$ mm from the tube transition were estimated using the scaling relationship [24] and the current density for the larger diameter tube section, 2.6 cm. No values for the reduced electric field were determined for the axial positions between $+4$ and $+10$ mm. As stated previously, the electron density is greater in the small diameter tube than in the wider diameter tube but this decrease with axial position, past the tube diameter transition is not known. Although a constant electron density was used inside the small diameter tube and up to an axial position 4 mm past the diameter transition for the reasons given above, estimates of the electron densities for the axial positions between 4 and 10 mm cannot be made since the changing boundary conditions and discharge geometry cannot be quantified in the discharge cell. However, these axial positions are past the region of largest change in the metastable He density and also the double-layer region.

The reduced electric field axial profiles derived from the metastable He density profiles are shown in Fig. 7. The axial profiles with the cathode in the larger diameter tube are shown in Fig. 7(a), while those shown in Fig. 7(b) are for the anode in the wide tube section. The axial E/n profile goes through a maximum in the region of the double layer at the diameter transition when the cathode is in the wider tube section. It has been known for some time that a plasma sac (and multiple space-charge layer) forms when the cathode is in the wider tube section of an abrupt diameter transition in a discharge [6,12,13,21]. Andrews and Allen [6] suggested that a double layer is formed in this case for the following reason. Even though the reduced electric field is greater in the smaller diameter tube [24], the electron density in this tube is also greater than in the wide section because the increased electron drift velocity [25] (due to higher E/n) is not sufficient to maintain current continuity. Since the ratio of the ion loss rate to the production rate increases in the smaller diameter tube, electrons moving into the smaller diameter tube from the wide section must acquire more energy to increase the ionization rate for the discharge to remain quasineutral. Because of the interdependency of the reduced electric field, electron density, and the rate of ionization, these parameters are considered collectively. Therefore, the local electric field goes through a maximum in the region of the double layer to increase the energy of the electrons entering the smaller diameter tube when the cathode is in the larger diameter tube. For the opposite polarity condition with the anode in the larger diameter tube, no measurable maximum exists in the axial E/n profile. The reduced electric field and electron density decrease in the wide tube section and the ratio of the ion loss rate to the production rate decreases. The electrons moving into the wide section do not necessarily require more

energy to maintain quasineutrality. Thus, when the anode is in the larger diameter tube, the double layer is weaker. A simple, self-consistent explaination for the difference with discharge polarity of the axial profile of the reduced electric field near the diameter transition could be that the electric fields are additive in one case and subtractive in the other while satisfying current continuity requirements imposed by the diameter discontinuity of the positive column. The local increase in the electric field would then be stronger when the cathode is in the larger diameter tube than when the anode is in the wide section.

V. CONCLUSION

The line-integrated, metastable He $2\,^3S_1$ population density profile in the region of a double layer formed at an abrupt tube diameter transition was measured by diode-laser absorption spectroscopy. The triplet metastable He axial profile showed an enhanced production in the region of the double layer when the cathode was in the large diameter tube section of the discharge. Axial profiles of E/n were estimated from the metastable He density profiles with a triplet metastable He balance equation, assuming that the eedf is in equilibrium with the reduced electric field. The E/n axial profile rises to a maximum when the cathode is in the large diameter tube in the vicinity of the diameter transition with a (multiple space-charge) double layer, while the E/n axial profile when the anode is in the wider section has no measurable maximum, suggesting a much weaker space-charge layer. This discharge polarity dependence of the local reduced field may be due to the local field adding to the applied field in one polarity and subtracting from it in the opposite polarity.

ACKNOWLEDGMENTS

The authors would like to thank Dr. Alan Garscadden for suggesting the discharge configuration for static double-layer formation, Dr. Charlie DeJoseph for many useful discussions, and Mr. Alan Forlines for technical support. One of the authors (J.M.W.) acknowledges support under USAF Contract No. F33615-98-C-2806.

[1] H. S. Maciel and J. E. Allen, J. Plasma Phys. **42**, 321 (1989).
[2] M. A. Raadu and J. J. Rasmussen, Astrophys. Space Sci. **144**, 43 (1988).
[3] J. I. Khan, Proc. Astron. Soc. Aust. **8**, 29 (1989).
[4] G. Hairapetian and R. L. Stenzel, Phys. Rev. Lett. **65**, 175 (1990).
[5] V. Lapuerta and E. Ahedo, Phys. Plasmas **7**, 2693 (2000).
[6] J. G. Andrews and J. E. Allen, Proc. R. Soc. London, Ser. A **320**, 459 (1971).
[7] J. S. Levine and F. W. Crawford, J. Plasma Phys. **24**, 359 (1980).
[8] N. Hershkowitz, Space Sci. Rev. **41**, 351 (1985).
[9] B. Song, N. D'Angelo, and R. L. Merlino, J. Phys. D **24**, 1789 (1991).
[10] S. Torvén, J. Appl. Phys. **49**, 2563 (1978).
[11] M. A. Raadu, Phys. Rep. **178**, 25 (1989).
[12] F. W. Crawford and I. L. Freeston, in *Proceedings of the 6th International Conference on Phenomena in Ionized Gases* (SERMA, North-Holland, Amsterdam, 1963), pp. 461–464.
[13] M. F. Hoyaux and E. M. Williams, J. Appl. Phys. **38**, 3630 (1967).
[14] S. Sandahl, Phys. Scr. **3**, 275 (1971).
[15] M. W. Millard, P. P. Yaney, B. N. Ganguly, and C. A. DeJoseph, Plasma Sources Sci. Technol. **7**, 389 (1998).
[16] P. A. Miller, J. T. Verdeyen, and B. E. Cherrington, Phys. Rev. A **4**, 692 (1971).
[17] H. Okabe, *Photochemistry of Small Molecules* (Wiley-Interscience, Toronto, 1978), p. 42.
[18] J. T. Verdeyen, in *Laser Electronics* (Prentice-Hall, Englewood Cliffs, NJ, 1981), Chap. 7.
[19] W. L. Weise, M. W. Smith, and B. M. Glennon, *Atomic Transition Probabilities*, Natl. Bur. Stand. Publ. No. NSRDS-NBS4 (US GPO, Washington, D.C., 1966), Vol. 1.
[20] A. von Engel, *Ionized Gases* (American Institute of Physics, New York, 1994), Chap. 8 (originally published by Oxford University Press, 1965).
[21] D. Andersson, J. Phys. D **10**, 1549 (1977).
[22] E. A. D. Hartog, T. R. O'Brian, and J. E. Lawler, Phys. Rev. Lett. **62**, 1500 (1989).
[23] A. V. Phelps, Phys. Rev. **99**, 1307 (1955).
[24] B. E. Cherrington, IEEE Trans. Electron Devices **26**, 148 (1979).
[25] S. C. Brown, *Basic Data of Plasma Physics, 1966* (MIT Press, Cambridge, 1967).
[26] A. V. Phelps and J. P. Molnar, Phys. Rev. **89**, 1202 (1953).